Shear melting of confined solid monolayer films

Martin Schoen
Institut für Experimentalphysik, Naturwissenschaftliche Fakultät, Universität Witten/Herdecke, Stockumer Str. 10, D-5810 Witten, Federal Republic of Germany

D. J. Diestler*
Richard B. Wetherill Laboratory of Chemistry, Purdue University, West Lafayette, Indiana 47907

John H. Cushman
Lilly Hall of Life Sciences, Purdue University, West Lafayette, Indiana 47907
(Received 25 November 1991; revised manuscript received 21 October 1992)

Strain-induced melting of solid phases in a prototypal slit pore [a monatomic fluid constrained between two plane-parallel walls made up like atoms fixed in the configuration of the (100) plane of the face-centered cubic lattice] is investigated by Monte Carlo calculations in the "isostress-isostrain" ensemble where the thermodynamic state of the pore phase is uniquely determined by a fixed number of molecules, constant load or normal stress and constant temperature. If the walls are properly aligned laterally, a commensurate solid phase can form epitaxially. Moving the walls out of alignment (shear strain) creates a distorted solid, which reacts (shear stress) by tending to realign the walls. If the shear strain is increased beyond a critical value, the solid begins to melt. However, melting is a continuous transition which does not immediately lead to a normal liquid, but rather a disordered phase that sustains a non-negligible shear stress. Shear melting is contrasted to ordinary melting at constant normal stress, which appears to be a first-order transition.

I. INTRODUCTION

Fluids confined to spaces of molecular dimension by solid surfaces (vicinal fluids) play a vital role in such diverse phenomena as lubrication,[1] swelling of clay soils,[2] and transport in biological membranes.[3] Relatively recent technological advances have made the more or less direct microscopic examination of vicinal fluids possible. In particular, the development of the surface forces apparatus (SFA)[4–6] over the last decade has permitted measurement of the forces acting between plane-parallel solid surfaces (walls) separated by molecularly thin layers of fluid. The vicinal fluid is maintained in thermodynamic equilibrium with bulk fluid at fixed temperature and pressure. The molecular structure of the walls is well characterized (usually atomically smooth mica). The walls are attached to springs that can be electrically and mechanically manipulated to control precisely the applied stresses. In the latest version of the SFA[5] only normal strain (i.e., wall separation in the z direction) and shear strain (i.e., alignment of walls in the x direction) and their conjugate stresses are measured.

The behavior of the vicinal phase is studied theoretically by statistical thermodynamics. The complexity of even the simplest models precludes analytical treatment. However, powerful electronic computers permit simulation of realistic models by means of Monte Carlo (MC) and molecular dynamics (MD) methods. Computer simulations are essentially *virtual* experiments on the molecular scale. They are conducted within the framework of a particular statistical-mechanical ensemble, which is characterized by a given set of parameters, namely, a set of thermodynamic variables sufficient in number to specify uniquely the thermodynamic state. Since all ensembles are equivalent in the thermodynamic limit, the choice of ensemble can, in principle, be made out of convenience to the simulator (i.e., virtual experimenter). If one wished to mimic the SFA, for example, one would choose a "grand-isostress" ensemble where the parameters are the thermodynamic variables controlled by the SFA: chemical potential, μ; temperature, T; normal stress, or load; shear stress; plus additional "complementary" stresses or strains. This ensemble will be further discussed in Sec. VII. Simply mimicking the SFA is, of course, useful in interpreting data or suggesting additional measurements. Mere mimicking nevertheless fails to take advantage of the great versatility of virtual experiments: they can be performed in any ensemble. By exploring the behavior of the vicinal phase in ensembles not realizable in the laboratory, the virtual experimenter gleans information not accessible to the "real" experimenter. The virtual data complement the real data and together they can provide a deeper understanding of the nature of the vicinal phase than either one alone could provide. It is in this spirit that we have conducted the isostress-isostrain ensemble MC study for thin vicinal layers to be presented here.

By means of the SFA, the normal force (solvation force) between the walls has been shown to oscillate between attraction and repulsion as the separation varies. The period of this oscillation is of the order of the diameter of a fluid molecule, which suggests that whole layers of fluid are transferred between bulk and vicinal phases. Thus, although the SFA measurements provide no direct information on the structure of the vicinal fluid, they suggest that it is ordered in discrete layers parallel with the walls. This hypothesis is given credibility by the form of

the local density obtained for vicinal fluid models by integral equations[7,8] and computer simulation.[9–11]

It had not been appreciated until recently that the molecular structure of the walls has a profound influence on the behavior of vicinal fluids.[11,12] Depending upon the structure and alignment of the walls, the vicinal fluid can freeze and thaw periodically as the separation between the walls changes. The finding of periodic formation of a solid phase in computer simulations[11–15] of model vicinal fluids is now invoked[5,16,17] to explain the abrupt periodic transition between lateral "stick" and "slip" motion observed in the SFA[4–6] when the walls are slid past one another under constant normal load. In order to initiate sliding, a critical shear stress must be overcome. Sliding then continues with the walls moving at constant relative speed.

Shear melting of vicinal phases was first simulated in a prototypic model, consisting of a monatomic fluid constrained between fcc (100) walls of like atoms, by means of the grand-canonical ensemble MC, where T, μ, and wall separation h are held fixed, as the shear strain is varied.[13] Employment of the MC method takes cognizance of the extremely low relative speed [$\sim 10^{-9}$ Å/ps (Ref. 6)] of the walls in the SFA. Sliding is represented as a quasistatic process, that is, as a succession of equilibrium states, each state being specified by a particular fixed lateral alignment of the walls. Because of the wall structure each alignment has an associated shear strain, expressible quantitatively in terms of the dimensions of the unit cell of the wall. Equilibrium properties of the vicinal phase are then obtained as a function of the shear strain, other thermodynamic variables being held fixed. Perhaps the most interesting such property is the shear stress τ_4 sustained by the vicinal phase, that is, the force per unit area acting transversely (in the x direction) on the walls. If, for example, the walls are aligned initially so that the vicinal phase is solid, τ_4 increases roughly linearly with strain until a critical value is reached, beyond which the vicinal solid abruptly melts. Since the grand-canonical ensemble describes an open system, melting is accompanied by drainage. It is noteworthy that the transition is discontinuous and that the newly formed vicinal phase is not truly fluidic, since it supports a residual shear stress.

Under certain conditions drainage appears not to occur as the walls are slid.[17] In such circumstances it is convenient to employ an "isostress-isostrain" ensemble in which the number of vicinal molecules, N, is fixed, along with normal stress τ_3, T, and the remaining strains, except the shear strain, which is systematically varied. A simulation along these lines has been carried out by Thompson and Robbins,[15] who used nonequilibrium MD to study the shearing behavior of a monatomic fluid confined between fcc (111) walls under a constant load. One wall is attached to a spring which is attached in turn to a translation stage that moves in the x direction at uniform speed. They found that below a critical speed the fluid freezes and thaws periodically, the walls exhibiting the corresponding stick-slip movement described above. If the speed is too great, the highly cooperative process of freezing does not have time to occur and the walls glide freely over one another. It should be pointed out that the speeds used in this simulation are about nine orders of magnitude greater than the typical speeds employed in the SFA.

Very recently Lupkowski and van Swol[18] performed a dynamical simulation within a "grand-isostress" ensemble, where μ, τ_3, and T are held fixed as the shear strain is varied. They applied a novel grand-canonical MD technique to the prototypic slit pore comprising fcc(100) walls confining atomic fluid at constant load. One wall is attached to a spring whose other end is fixed. The other wall is translated in the x direction at uniform speed. The shear strain in the y direction is apparently held fixed. The observation of Lupkowski and van Swol is similar to that of Thompson and Robbins,[15] that is, stick-slip motion, accompanied by drainage, at sufficiently low shear rate. Again, however, the lowest shear rate is nine orders of magnitude greater than actual SFA rates.

Instead of attempting to incorporate the walls dynamically, we again invoke the extremely low relative wall speed to justify use of the MC method. Thus, the point of this article is to present the results of a MC study of shear melting in the prototypic model for vicinal fluids within the context of the "isostress-isostrain" ensemble. We restrict attention to monolayer films, for which shear melting appears to be a continuous transition. During melting, the vicinal phase becomes strongly anisotropic as it is sheared preferentially in the x direction. Especially intriguing is the nature of the "molten" vicinal phase, which, although highly disordered, is not a simple fluid, as it supports a shear stress.

II. MODEL OF THE VICINAL SYSTEM

In our basic model N (vicinal) rare-gas atoms are confined between two walls. Each wall consists of a square "unit cell" of the (100) plane of a face-centered-cubic (fcc) lattice (see Fig. 1); the length of the side of the square is s. Each wall comprises N_S rigidly fixed rare-gas atoms at a surface density $d_S \equiv N_S/s^2$. The walls are taken parallel to one another and perpendicular to the z axis (see Fig. 2). We shall refer to this model as the prototypical structured slit pore or simply the prototype. Coordinates of atoms in the walls are related by

$$\begin{aligned} x_i^{(2)} &= x_i^{(1)} + \alpha l \ , \\ y_i^{(2)} &= y_i^{(1)} \ , \\ z_i^{(2)} &= z_i^{(1)} + h \ , \quad i = 1, \ldots, N_S \ , \end{aligned} \tag{1}$$

where the superscripts (1) and (2) refer to the lower ($z_i^{(1)}=0$) and upper walls, respectively. l is the lattice constant and α is the registry parameter. Note that the current version of the prototype permits variations of registry only in the x direction. If $\alpha=0.0$, the walls are in registry (i.e., they correspond to alternate layers of a three-dimensional fcc lattice); if $\alpha=0.5$, the walls are out of registry (i.e., upper and lower walls correspond to adjacent layers of the fcc lattice, see Fig. 1). The parameter α is a measure of shear strain in the x direction on planes of

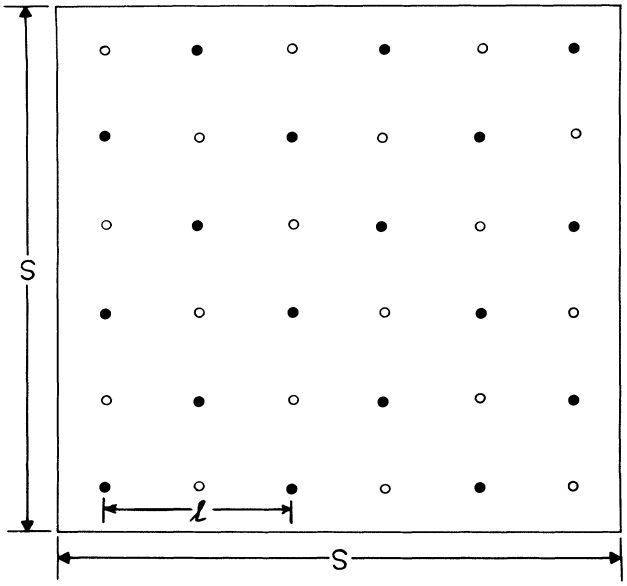

FIG. 1. Square unit cell of the (100) plane of the fcc lattice. Filled and open circles represent atom in pore walls at $z=0$ and $z=h$ [see Eq. (1)]; l is the lattice constant; here $\alpha=0.5$.

constant z. We impose the usual periodic boundary conditions in the x and y directions.

The total configurational (potential) energy of the system is written as

$$U=U_{FF}+U_{FS}^{(1)}+U_{FS}^{(2)} , \tag{2}$$

where

$$U_{FF}=\sum_{i=1}^{N-1}\sum_{j>i}^{N} u(r_{ij}) \tag{3a}$$

and

$$U_{FS}^{(k)}=\sum_{i=1}^{N}\sum_{j=1}^{N_S} u(r_{ij}^{(k)}) \quad k=1,2 \tag{3b}$$

are the fluid-fluid (FF) and fluid-wall (FS) contributions. The superscripts (1) and (2) refer again to the walls at $z=0$ and $z=h$, respectively. All interatomic interactions $u(r_{ij})$ are assumed to be of the Lennard-Jones (12,6) form

$$u(r)=4\epsilon[(\sigma/r)^{12}-(\sigma/r)^{6}] . \tag{4}$$

In addition to the pairwise fluid-wall interactions $U_{\rm FS}^{(k)}$, all fluid atoms are subject to an infinite square-well background potential [$u(z)=\infty, z<0, z>h$; $u(z)=0, 0\le z\le h$] so that they are strictly confined to the range $0\le z\le h$.

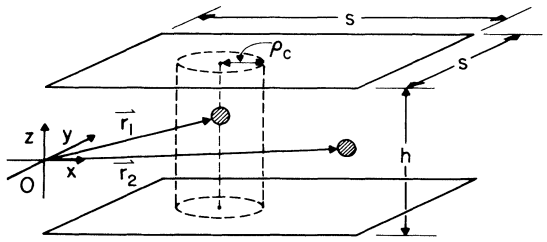

FIG. 2. Schematic of prototypal slit pore showing planes of walls and cutoff cylinder.

III. STATISTICAL THERMODYNAMICS OF THE SLIT PORE IN THE ISOSTRESS-ISOSTRAIN ENSEMBLE

The internal energy U of a pure bulk (homogeneous) fluid can, in principle, be expressed as a unique function of the entropy S, volume V, and number of molecules N. In the case of the slit pore, however, the rigid walls impose an external field on the vicinal phase, so that additional extensive variables must be specified in order to fix uniquely the internal energy. These variables are controlled by relative movements of the walls, which are of two types: compression and shear. The degree of compression is altered by changing h or, by means of "pistons," the distances between imaginary planes (say between $x=0$ and $x=s_x$ or between $y=0$ and $y=s_y$) that bound the phase in the x and y directions. The extent of shear is controlled by the registry parameters. Note that for all results presented in Sec. VI, $s_x=s_y=s$.

The movements of the walls can be described quantitatively through the displacement gradients[19–21] which can be expressed in terms of the dimensions of the pore as

$$\begin{aligned}
\sigma_1&=u_{xx}=(s_x-s_x^0)/s_x^0 ,\\
\sigma_2&=u_{yy}=(s_y-s_y^0)/s_y^0 ,\\
\sigma_3&=u_{zz}=(h-h^0)/h^0 ,\\
\sigma_4&=u_{xz}=\alpha l/h^0 ,
\end{aligned} \tag{5}$$

where the superscript null refers to the reference state. The displacement gradients $u_{\alpha\beta}$ describe the relative separation of elements of mass under a prescribed strain. Thus, if two mass elements are separated by the vector $\mathbf{r}^0$ in the reference state, then they are separated in the strained state by vector $\mathbf{r}$, which is related to $\mathbf{r}^0$ by

$$\underline{r}=(\underline{\underline{1}}+\underline{\underline{u}})\underline{r}^0 . \tag{6}$$

In Eq. (6) $\underline{r}$ and $\underline{r}^0$ represent column vectors whose elements are the Cartesian components of the corresponding vectors and $\underline{\underline{1}}$ and $\underline{\underline{u}}$ are matrices whose α,β elements are $\delta_{\alpha\beta}$ (the Kronecker delta) and $u_{\alpha\beta}$, respectively. Note that under infinitesimal stains the volume of the strained vicinal phase can be related to the volume V^0 of the reference phase by

$$V=V^0(1+\sigma_1+\sigma_2+\sigma_3)=V^0(1+\mathrm{Tr}\underline{\underline{u}}) . \tag{7}$$

The work done by the vicinal phase against the applied stresses during an infinitesimal distortion is given by

$$dW=-\sum_i \tau_i d(V^0\sigma_i) . \tag{8}$$

The notation for the stresses τ_i parallels that for the strains:

$$\tau_1 = T_{xx} ,$$
$$\tau_2 = T_{yy} ,$$
$$\tau_3 = T_{zz} , \tag{9}$$
$$\tau_4 = T_{xz} ,$$

where $T_{\alpha\beta}$ is the αth (Cartesian) component of the force acting on a unit area pointing in the β direction. The combined first and second laws of thermodynamics for the prototype can thus be expressed

$$dU = TdS + \sum_i \tau_i d(V^0\sigma_i) + \mu dN , \tag{10}$$

from which we infer that the internal energy is a unique function of the following extensive variables: $S, N, \{V^0\sigma_i\}_{i=1}^4$.

The virtual experiment that we wish to model holds the temperature T, number of molecules N, normal stress τ_3, and strain components σ_1, σ_2, and σ_4 constant. It is therefore convenient to introduce the thermodynamic potential defined by

$$\mathcal{G} = U - TS - \tau_3 V^0\sigma_3 , \tag{11}$$

which is analogous to the usual Gibbs free energy defined for bulk phases. From Eqs. (10) and (11) we obtain

$$d\mathcal{G} = -SdT - V^0\sigma_3 d\tau_3 + \mu dN + \sum_{j\neq 3} \tau_j d(V^0\sigma_j) . \tag{12}$$

Thus, $\mathcal{G} = \mathcal{G}(T, N, \tau_3, \sigma_3')$ and we have from Eq. (12)

$$S = -(\partial\mathcal{G}/\partial T)_{N,\tau_3,\sigma_3'} ,$$
$$\sigma_3 = -V^{0-1}(\partial\mathcal{G}/\partial\tau_3)_{T,N,\sigma_3'} ,$$
$$\mu = (\partial\mathcal{G}/\partial N)_{T,\tau_3,\sigma_3'} , \tag{13}$$
$$\tau_i = V^{0-1}(\partial\mathcal{G}/\partial\sigma_i)_{T,N,\tau_3,\sigma_{3,i}'} \quad i\neq 3 ,$$

where the abbreviations σ_3' and $\sigma_{3,i}'$ stand for the sets $\{\sigma_i\}_{i\neq 3}$ and $\{\sigma_j\}_{j\neq 3,i}$.

Following the approach originated by Schrödinger[22] and extended by Hill[23] and by McQuarrie,[24] we find the characteristic potential for the isostress-isostrain ensemble

$$\mathcal{G} = -k_B T \ln\Delta , \tag{14}$$

where Δ is the partition function. Then using the thermodynamic relations given in Eqs. (13) and the statistical-mechanical expressions in (14), we obtain

$$S = k_B \ln\Delta + k_B T(\partial \ln\Delta/\partial T)_{N,\tau_3,\sigma_3'} ,$$
$$\mu = \langle\mu\rangle = -k_B T(\partial \ln\Delta/\partial N)_{T,\tau_3,\sigma_3'} ,$$
$$V^0\sigma_3 = \langle V^0\sigma_3\rangle = k_B T(\partial \ln\Delta/\partial\tau_3)_{T,N,\sigma_3'} ,$$
$$\tau_i = \langle\tau_i\rangle = -k_B T[\partial \ln\Delta/\partial(V^0\sigma_i)]_{T,N,\tau_3,\sigma_{3,i}'} , \quad i\neq 3 \tag{15}$$

where the angular brackets signify a statistical-mechanical average.

In the classical limit, the partition function becomes

$$\Delta = \sum_{\sigma_3} Q(N,T,\sigma)\exp(\tau_3 V^0\sigma_3/k_B T) , \tag{16}$$

where the canonical partition function is

$$Q = Z_N/(N!\Lambda^{3N}) \tag{17}$$

and the configurational integral is

$$Z_N = \int_V d\mathbf{r}^N \exp[-U(\mathbf{r}^N;\sigma)/k_B T] . \tag{18}$$

The symbol σ denotes the set of strains $\{\sigma_i\}_{i=1}^4$. In Eq. (18) $\mathbf{r}^N = \{\mathbf{r}_1, \mathbf{r}_2, \ldots \mathbf{r}_N\}$ denotes a $3N$-dimensional point in configuration space and $d\mathbf{r}^N = \prod_{i=1}^N d\mathbf{r}_i$ is the corresponding hypervolume element. The implicit dependence of the configurational energy $U(\mathbf{r}^N;\sigma)$ on N and σ is indicated. The thermal de Broglie wavelength is defined by

$$\Lambda \equiv (h^2/2\pi m k_B T)^{1/2} , \tag{19}$$

where m is the mass of an atom, h is Planck's constant, and k_B is Boltzmann's constant. The mean value of an observable O can be expressed as

$$\langle O\rangle = \sum_{\sigma_3} \int_V d\mathbf{r}^N P(\mathbf{r}^N;\sigma) O(\mathbf{r}^N;\sigma)$$
$$= \frac{\sum_{\sigma_3} \exp(\tau_3 V^0\sigma_3/k_B T) \int_V d\mathbf{r}^N \exp[-U(\mathbf{r}^N;\sigma)/k_B T] O(\mathbf{r}^N;\sigma)}{\sum_{\sigma_3} \exp(\tau_3 V^0\sigma_3/k_B T) \int_V d\mathbf{r}^N \exp[-U(\mathbf{r}^N;\sigma)/k_B T]} , \tag{20}$$

Equation (20) defines the classical distribution function $P(\mathbf{r}^N;\sigma)$. Note that the volume of integration V depends implicitly on σ via Eq. (7). Substituting Eq. (5) for σ_3 into (20) and simplifying the result gives

$$\langle O\rangle = \frac{\int dh \exp(\tau_3 s^2 h/k_B T) \int_V d\mathbf{r}^N \exp[-U(\mathbf{r}^N;\sigma)/k_B T] O(\mathbf{r}^N;\sigma)}{\int dh \exp(\tau_3 s^2 h/k_B T) \int_V d\mathbf{r}^N \exp[-U(\mathbf{r}^N;\sigma)/k_B T]} . \tag{21}$$

In arriving at Eq. (21), we have used the relation $V^0 = s^2 h^0$, since $s_x^0 = s_y^0 = s$ is fixed. We have also replaced the sum on σ_3 by an integral on h, taking the wall separation to be a continuous variable.

IV. MONTE CARLO CALCULATIONS IN THE ISOSTRESS-ISOSTRAIN ENSEMBLE

Before discussing the numerical aspects of MC in the (N,τ_3,T) ensemble, we note that the integration over configuration space in Eq. (21) involves a density of states that depends on h. This dependence can be made explicit by introducing the transformation

$$\underline{r}_i' = \begin{bmatrix} x_i' \\ y_i' \\ z_i' \end{bmatrix} = \begin{bmatrix} x_i/s \\ y_i/s \\ z_i/h \end{bmatrix}, \quad i=1,2,\ldots N \ . \tag{22}$$

Then Eq. (21) assumes the form

$$\langle O \rangle = \frac{\int dh \exp(\tau_3 s^2 h/k_B T) h^N \int_{V'} d\mathbf{r}'^N \exp[-U(\mathbf{r}'^N;\sigma)/k_B T] O(r'^N;\sigma)}{\int dh \exp(\tau_3 s^2 h/k_B T) h^N \int_{V'} d\mathbf{r}'^N \exp[-U(\mathbf{r}'^N;\sigma)/k_B T]} \ , \tag{23}$$

where the configurational integral now extends over the unit hypercube V'. From Eq. (23) it is clear that the Markov chain resulting from MC must be characterized by a limiting probability distribution proportional to

$$\exp\{[\tau_3 s^2 h - U(\mathbf{r}'^N;\sigma)]/k_B T + N \ln h\} \ . \tag{24}$$

The sampling problems associated with a changing density of states were emphasized by Vorontsov-Vel'Yaninov *et al.*[25] in the context of isobaric-isothermal (N,p,T) ensemble MC, where one allows fluctuations in the volume rather than just h. Finn and Monson[26] employed an isostress-isostrain MC technique to study the prewetting transition in smooth-walled slit pores, but they do not mention sampling problems connected with variations in h.

To implement the MC method for the (N,τ_3,T) ensemble, we modify the algorithm first suggested by Metropolis *et al.*[27] The Markov chain is initiated by placing N atoms in a suitable starting configuration (see Table I). It is then propagated as a sequence of pairs of consecutive steps. Because of the relation between Δ and Z_N [see Eqs. (16)–(18)] the first of the two steps is identical with that of the original Metropolis scheme for MC in the canonical ensemble.[28] We employ the minimum image convention and a cylindrical cutoff for the interactions (see Fig. 2).

In the second MC step h is changed to a new (trial) value given by

$$h_n = h_o + \delta_h(2\xi - 1) \ , \tag{25}$$

where ξ is a pseudorandom number from a uniform distribution on [0,1] and δ_h is the maximum displacement. The value of δ_h is adjusted (see Table I) during the MC run so that 40–50% of all attempts to change h are accepted according to the probability

$$P_2 = \begin{cases} 1, & B \geq 1 \\ B, & B < 1 \end{cases} \tag{26}$$

where the pseudo-Boltzmann factor is given by

$$B = \exp\{[\tau_3 s^2 \Delta h - \Delta U]/k_B T + N \ln(h_n/h_o)\} \tag{27}$$

and $\Delta h = h_n - h_o$. To compute ΔU caused by the change in h,z coordinates of all atoms (vicinal plus wall) are scaled by h_n/h_o, which necessitates a calculation of U from Eqs. (2)–(4) twice per MC step. Note that a full evaluation of the double sums in Eqs. (3a) and (3b) is unavoidable because *all* atoms assume new positions when h_o changes to h_n. This is unlike the canonical step, where only *one* atom is moved at a time so that only single sums survive in Eqs. (3a) and (3b). Since h changes during the

TABLE I. Parameters of MC calculations in the (N,τ_3,T) ensemble.

Side of wall	$s = 7.9925\sigma,\ 25.576\sigma$
Density of atoms in wall	$d_s = 0.78272/\sigma^2$
Starting configuration	random ($\alpha = 0.0$)
	last configuration of run at previous α ($\alpha > 0.0$)
Maximum displacement of atom	$\delta = 0.05\sigma - 0.08\sigma$
Maximum displacement of wall	$\delta_h = 0.10\sigma - 0.15\sigma$
Number of equilibration steps	10^5
Numbers of atoms	$N = N_S = 50,512$
Number of steps between configurations included in ensemble averages	$2N$ (thermodynamic properties)
	N (local density)
	$10N$ (pair-correlation function)
Total number of MC steps	10^7 ($N=50$), 1.5×10^7 ($N=512$)
Radius of cutoff cylinder	$\rho_c = 3.5\sigma$
Thickness $\Delta\rho_{12}$ of annulus used to compute $g^{(2)}(z_1,\rho_{12})$	0.02σ

second step of the MC procedure, ΔU must be corrected for changes in the singlet and pair distribution functions $\rho^{(1)}(\mathbf{r}_1)$ and $\rho^{(2)}(\mathbf{r}_1,\mathbf{r}_2)$; by the uniform density approximation[11] it is straightforward to compute this correction from Eqs. (A6)–(A10) given in the appendix of Ref. 11.

V. PROPERTIES OF THE VICINAL PHASE

Since we restrict our consideration here to monolayer films, a sufficient description of the film's structure is given by the in-plane pair-correlation function $g^{(2)}$,

$$g^{(2)}(\rho_{12})=\langle N(\rho_{12})\rangle/2\pi\rho_{12}\Delta\rho_{12}\Delta z_{12}\rho^{(1)} , \tag{28}$$

where $\langle N(\rho_{12})\rangle$ is the mean number of atoms in an annulus of radius ρ_{12}, width $\Delta\rho_{12}$ (see Table I), and height Δz_{12} centered on a reference atom (1). Δz_{12} is taken equal to the thickness of the monolayer, which is determined from the local density $\rho^{(1)}$, as detailed in Ref. 11.

Beginning with Eq. (15) one can straightforwardly, albeit tediously, derive explicit molecular expressions for the stress components. Separating the compressional components into fluid-fluid and fluid-wall contributions, one finds

$$\langle\tau_\alpha\rangle=\langle\tau_{\alpha,FF}\rangle+\langle\tau_{\alpha,FS}\rangle , \tag{29}$$

where

$$\langle\tau_{\alpha,FF}\rangle=-Nk_BT\langle h^{-1}\rangle/s^2 +(s^2\langle h\rangle)^{-1}\left\langle\sum_{i=1}^{N-1}\sum_{j>i}^{N}\frac{du}{dr_{ij}}\frac{\alpha_{ij}^2}{r_{ij}}\right\rangle \tag{30a}$$

and

$$\langle\tau_{\alpha,FS}\rangle=(s^2\langle h\rangle)^{-1} \times\left\langle\sum_{k=1}^{2}\sum_{i=1}^{N}\sum_{j=1}^{N_S}\frac{du}{dr_{ij}^{(k)}}\frac{\alpha_{ij}^{(k)2}}{r_{ij}^{(k)}}\right\rangle , \tag{30b}$$

and $\alpha=x(1),y(2)$. The shear-stress components are given by

$$\langle\tau_4\rangle=-s^{-2}\left\langle\sum_{i=1}^{N}\sum_{j=1}^{N_S}\frac{du}{dr_{ij}^{(2)}}\frac{x_{ij}^{(2)}}{r_{ij}^{(2)}}\right\rangle . \tag{31}$$

The latter form is especially transparent: $s^2\langle\tau_4\rangle$ is just the negative of the average value of the x component of the force exerted on wall (2) by the vicinal phase. That is,

$$s^2\langle\tau_4\rangle=-\langle F_x^{(2)}\rangle=\left\langle\sum_{j=1}^{N_S}\frac{\partial U_{FS}^{(2)}}{\partial x_j}\right\rangle . \tag{32}$$

By symmetry, the force acting on wall (1) should be equal in magnitude but opposite in sign. That is,

$$s^2\langle\tau_4\rangle=\langle F_x^{(1)}\rangle . \tag{33}$$

The alternative expressions [Eqs. (32) and (33)] for $\langle\tau_4\rangle$ provide a check on the consistency of the computations.

By reasoning similar to the above we conclude that $s^2\tau_3$ should be the negative of the z component of the force exerted on the walls by the vicinal phase. Thus,

$$\begin{aligned}\tau_3&=-s^{-2}\langle F_z^{(2)}\rangle\\&=-s^{-2}\left\langle\sum_{i=1}^{N}\sum_{j=1}^{N_S}\frac{du}{dr_{ij}^{(2)}}\frac{z_{ij}^{(2)}}{r_{ij}^{(2)}}\right\rangle\\&=s^{-2}\langle F_z^{(1)}\rangle ,\end{aligned} \tag{34}$$

where the third line follows by symmetry arguments. To check that the average normal stress on the walls agrees with the value τ_3 input, we compute the quantity

$$\bar{\tau}_3\equiv(\langle F_z^{(1)}\rangle-\langle F_z^{(2)}\rangle)/2s^2 . \tag{35}$$

VI. RESULTS

To validate our MC procedure we compare our results with results previously obtained from MC calculations in the grand-canonical ensemble, in which the thermodynamic state of the pore phase is determined by fixed values of μ, $V=s^2h$, and T.[11] For a number of states we computed the average number of vicinal atoms $\langle N\rangle$, the fluid-fluid and fluid-wall contributions to the configurational per particle energy $\langle U/N\rangle$, $\langle\tau_3\rangle$, and $\bar{\tau}_3$ (see Table VII in Ref. 11). All numerical results are given in the customary dimensionless units defined in Table II. Note that in previous work we presented results for the "solvation force" f_s, also denoted previously by P_N, which is related to the normal stress τ_3 by $\langle\tau_3\rangle=-f_s$.

In the thermodynamic limit different ensembles are equivalent. Thus, the same thermodynamic state may be characterized by specifying either μ, V, and T in the grand-canonical ensemble or N, τ_3, and T in the isostress-isostrain ensemble. This permits us to take $\langle N\rangle$ and $\langle\tau_3\rangle$ from the previous MC calculations in the (μ,V,T) ensemble as the input N and τ_3 in the (N,τ_3,T) ensemble and compute the above-mentioned properties plus the average wall separation, $\langle h\rangle$, which is a fixed input parameter in the grand-canonical ensemble MC calculation.

The results for five different thermodynamic states are compiled in Table III together with the earlier results on the grand-canonical MC computation. The agreement between the configurational energy contributions $\langle U_{FF}\rangle$ and $\langle U_{FS}\rangle$ in the two ensembles is better than 1% in all cases. The discrepancy between τ_3 input and $\bar{\tau}_3$ computed by Eq. (35) can be as large as 16% (state 3), although it is less, the larger the value of τ_3. An inspection of Table VII in Ref. 11 reveals that for state 3, fluid-fluid and fluid-wall contributions to $\bar{\tau}_3$ nearly cancel. This particular state is therefore more prone to the usual numerical problems associated with differences between large

TABLE II. Reduced variables ($\sigma=3.405\times10^{-10}$m, $\epsilon/k_B=119.8$ K).

$h^*=h/\sigma$	$U^*=U/\epsilon$
$z^*=z/\sigma$	$T^*=k_BT/\epsilon$
$s^*=s/\sigma$	$\tau_i^*=\tau_i\sigma^3/\epsilon$
$\rho_{12}^*=\rho_{12}/\sigma$	

TABLE III. Comparison of results obtained from MC calculations in the grand-canonical ensemble[11] and the isostress-isostrain ensemble. N and τ_3^* form Ref. 11 are taken as input values in this work.

Source	State	N	$-\langle U_{FF}^*/N\rangle$	$-\langle U_{FS}^*/N\rangle$	$-\tau_3^*$	$-\bar{\tau}_3^*$	h^*	$\langle h^*\rangle$
Reference 11	1	51	2.180	5.929		7.20	1.85	
This work	1	51	2.172	5.889	7.20	7.23		1.85
Reference 11	2	53	2.230	5.947		0.70	2.00	
This work	2	53	2.216	5.891	0.70	0.73		2.00
Reference 11	3	53	2.330	5.489		0.16	2.10	
This work	3	53	2.326	5.334	0.16	0.19		2.11
Reference 11	4	135	4.037	2.862		4.03	3.40	
This work	4	135	4.038	2.857	4.03	4.15		3.40
Reference 11	5	151	4.278	2.546		0.80	3.80	
This work	5	151	4.307	2.571	0.80	0.89		3.78

numbers of about the same magnitude than are most of the other states considered here. Similar concerns apply to state 5, but for all other states the deviation is less than 5%. The average wall separation $\langle h\rangle$ also agrees with h set in the grand-canonical calculations to better than 1%.

In the (μ,V,T) ensemble, certain thermodynamically stable states have positive values of $\langle\tau_3\rangle$ (see Table VII in Ref. 11), which indicate that the walls are being pulled apart by the applied stress. In practice, the (N,τ_3,T) ensemble MC method breaks down in this case; $\langle h\rangle$ increase without bound. Although the precise cause is not clear, it appears to be a precarious balance among the terms of the argument of the pseudo Boltzmann factor B [Eq. (27)].

As demonstrated previously,[11] the vicinal fluid tends to freeze epitaxially in certain thermodynamic states. Since the structure of the vicinal solid is commensurate with the structure of the walls (Fig. 1), these states are characterized by $N=nN_S$, so that the number of solid layers is quantized. Depending on the registry parameter, $n=2k+1$ $(k=0,1,\ldots)$ for $\alpha=0.0$ or $n=2k$ $(k=1,2,\ldots)$ for $\alpha=0.5$. In the same way the wall separation h assumes characteristic values that are related to n and the lattice constant l (Fig. 1). From a random initial configuration with $N=50$, $d_s^*=0.78272$, $N_S=50$, $\alpha=0.0$, $T^*=1.0$, and $\tau_3^*=0.0$ a one-layer vicinal solid forms. Its structure is identified by the in-plane pair-correlation function $g^{(2)}$ [Eq. (28)], which reflects the order of a quasi-two-dimensional solid [Fig. 3(a)]. The x and y directions are equivalent, as indicated by $\langle\tau_1^*\rangle=\langle\tau_2^*\rangle=0.74$ and $\langle h^*\rangle=1.694$, which corresponds to a distance of 1.165σ between a vicinal atom and its four nearest neighbors in either wall. Note that this value is close to the minimum distance of $2^{1/6}\sigma$ of the Lennard-Jones (12,6) potential. Another measure of isotropy in the xy plane is provided by $\langle\tau_4\rangle$, which vanishes as it should for an unstrained solid phase.

This solid phase can be sheared by increasing the registry parameter from $\alpha=0.0$ to $\alpha=0.5$ in small steps of $\Delta\alpha=0.05$. The MC run for each $\alpha_i=(i-1)\Delta\alpha, i=2,\ldots,11$ is initiated from the final configuration of the previous MC run for α_{i-1}. The results are displayed in Fig. 4 for the stress components and the average separation between the walls. Note that at $\tau_3^*=0.0$, $\bar{\tau}_3^*$ [defined by Eq. (35)] ≈ 0.0 within error bars. The other stress components, however, exhibit an interesting dependence upon the shear strain. As α increases from 0.0, $\langle\tau_4\rangle$ increases approximately linearly until $\alpha\sim 0.10$. This is the expected response of an elastic solid to small strain. As α increases beyond 0.10, the *rate of increase* of $\langle\tau_4\rangle$ decreases markedly until $\langle\tau_4\rangle$ reaches a maximum at $\alpha\sim 0.18$, after which it decreases, eventually vanishing at $\alpha=0.5$, where the walls are completely out of registry. The transverse compressional stresses $\langle\tau_1\rangle$ and $\langle\tau_2\rangle$ are equal in the unstrained $(\alpha=0.0)$ isotropic monolayer. Shearing causes $\langle\tau_1\rangle$ to decrease with increasing α until a (relative) minimum is reached, which is very near the maximum in $\langle\tau_4\rangle$ at $\alpha\sim 0.18$. On the other hand, $\langle\tau_2\rangle$ increases with α to a (relative) maximum that roughly coincides with the minimum in $\langle\tau_1\rangle$. Beyond $\alpha\sim 0.3$, where we surmise the monolayer is molten, and therefore isotropic, $\langle\tau_1\rangle\simeq\langle\tau_2\rangle$.

The plots of $g^{(2)}$ in Fig. 3 suggest the complexity of melting as the vicinal solid is sheared. At $\alpha=0.0$, $g^{(2)}$ is strongly peaked, indicating a high degree of order. Structural characteristics are the second-neighbor shell peak at $\rho_{12}^*\approx 1.6$ and the overlapping peaks in the range $\rho_{12}^*\approx 2.3$–2.5, which are incompletely resolved because of thermal motion. The peak positions are identical to those associated with the (100) plane of the fcc lattice. At $\alpha=0.15$, the peaks at larger ρ_{12} are smoother. Nevertheless, the second-neighbor shell peak is still visible and so is a shoulder at $\rho_{12}^*\approx 2.3$, which is the remnant of the formerly unresolved double peak. Yet, the vicinal phase is still solidlike, as the sustained oscillations in $g^{(2)}$ at larger ρ_{12} indicate. At $\alpha=0.30$, however, the fcc features are no longer present in $g^{(2)}$. Most noticeable is the absence of a peak at $\rho_{12}^*\approx 1.6$ and the shift to smaller ρ_{12} for all peaks but the first. Although it is less pronounced than for smaller α, the peaked structure of $g^{(2)}$ indicates that solidlike character persists at $\alpha=0.3$. The dependence of $g^{(2)}$ on α suggests that melting occurs over the range $0.175<\alpha<0.35$.

As α increases further in the range $0.30\le\alpha\le 0.50$, the shear stress decreases continuously toward $\langle\tau_4^*\rangle=0.0$ at $\alpha=0.50$ (see Fig. 4). Once again it is instructive to compare $g^{(2)}$ for three different shear strains in this range [see Fig. 3(b)]. As above, we note the solidlike order reflected in $g^{(2)}$ at $\alpha=0.30$, which is the greatest strain at which $\langle\tau_1\rangle=\langle\tau_2\rangle$. If the strain is increased further, these stress components eventually become equal and the cor-

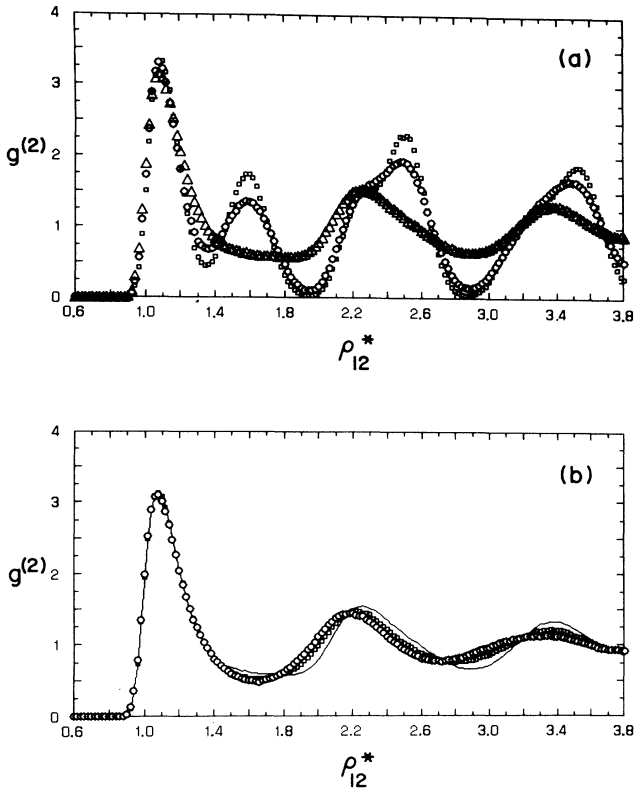

FIG. 3. In-plane pair-correlation functions for one-layer vicinal phase. (a) $\alpha=0.0(\square)$; $\alpha=0.15(\circ)$; $\alpha=0.30(\triangle)$. (b) $\alpha=0.30(-)$; $\alpha=0.35(\square)$; $\alpha=0.50(\circ)$.

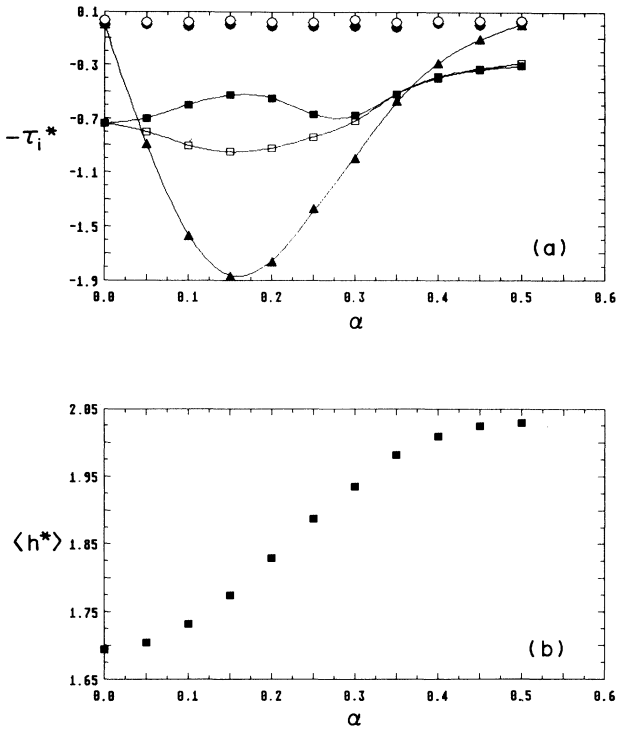

FIG. 4. (a) Negative stress components $-\tau_i^*$ as functions of α at $\tau_3^*=0.0$, $T^*=1.0$. $-\langle\tau_1^*\rangle(\blacksquare)$; $-\langle\tau_2^*\rangle(\square)$; $-\bar{\tau}_3^*(\circ)$; $-\langle\tau_4^*\rangle(\blacktriangle)$. To guide the eye, full lines are calculated from a cubic spline fit to the original data. (b) Average wall separation $\langle h^* \rangle$ as a function for α at $\tau_3^*=0.0$, $T^*=1.0$.

responding $g^{(2)}$ suggests a more disordered structure: peaks in $g^{(2)}$ are shifted to smaller interatomic separations and are more damped.

Comparing $g^{(2)}$ at $\alpha=0.35$ with that at $\alpha=0.50$, where the walls are completely out of registry, one is surprised that the structure of the vicinal phase seems to have changed little, since at the same time $\tau_{\|}=(\langle\tau_1\rangle+\langle\tau_2\rangle)/2$ changes by a factor of 1.73. Throughout the disordered regime $0.35\leq\alpha\leq0.50$, the vicinal phase exhibits a considerable shear stress. On the whole, the dependence of $g^{(2)}$ and the τ's on shear strain indicates that shear melting is a continuous transition. This is corroborated by the dependence of the average wall separation on α [Fig. 4(b)]. Starting from $\langle h^* \rangle\simeq1.70$ at $\alpha=0.0$, where the vicinal phase is a quasi-two-dimensional solid, $\langle h \rangle$ increases continuously by about 20%, until $\langle h^* \rangle\simeq2.03$, where the shear-free molten phase at $\alpha=0.50$ is reached.

The study of phase transitions by MC is difficult when such transitions are driven by highly cooperative long-range density fluctuations. Numerical results often show a substantial dependence on the size of the system, which renders suspect conclusions based on simulations of microscopic systems. The relevance of the microscopic results may, however, be tested to some extent by enlarging the MC sample. Table IV compares results for shear melting in slit pores with walls of two different areas. All the stress components agree within 3%,while the average wall separations deviate by less than 1%, irrespective of α. Thus, we believe that our results for the "smaller" pore ($s^*=7.9925$) already pertain to the thermodynamic limit.

None of the features discussed above depends qualitatively on temperature T or load τ_3, as can be seen from Fig. 5, where stress components are plotted as functions of α for a different load, $\tau_3^*=-0.24$, and two different temperatures, $T^*=1.00$ and 1.25. Increasing the load generally stabilizes the vicinal solid and leads to an increase of the maximum shear stress by about 8% based on the value for $\tau_3^*=0.0$. Similarly, the maximum difference between $\langle\tau_1\rangle$ and $\langle\tau_2\rangle$ increases by 25%, reflecting the enhanced ability of the vicinal solid to withstand applied strain under increased load. Both figures indicate that shear melting becomes more difficult with increasing normal stress. An increase in temperature, on the other hand, destabilizes the vicinal solid. This can be seen from Fig. 5(b) where again we plot various stress components as functions of applied shear strain at $\tau_3^*=-0.24$ and $T^*=1.25$. The destabilization may be seen in terms of the maxima in $\langle\tau_4\rangle$ and $(\langle\tau_1-\tau_2\rangle)$, which decrease by 35 and 50%, respectively, when the temperature is raised from $T^*=1.00$ to 1.25.

Although the continuous nature of shear melting appears to be unaffected by changes in load or temperature in the range studied, the character of the transition alters markedly if melting is effected by increasing temperature under constant load with no applied strain. This can be

TABLE IV. Effect of system size on shear melting of a one-layer vicinal solid at $T^*=1.0$, $\tau_3^*=-0.24$; System I: $N=N_S=50$, $s^*=7.9925$; System II: $N=N_S=512$, $s^*=25.576$.

System	α	$\langle h^* \rangle$	$-\langle \tau_1^* \rangle$	$-\langle \tau_2^* \rangle$	$-\bar{\tau}_3^*$	$-\langle \tau_4^* \rangle$
I	0.00	1.684	−0.672	−0.671	0.255	−0.003
II	0.00	1.682	−0.683	−0.687	0.253	−0.006
I	0.05	1.692	−0.633	−0.737	0.261	−0.971
II	0.05	1.693	−0.622	−0.729	0.255	−0.957
I	0.10	1.718	−0.531	−0.863	0.259	−1.725
II	0.10	1.720	−0.526	−0.857	0.251	−1.681
I	0.15	1.763	−0.403	−0.930	0.248	−2.014
II	0.15	1.760	−0.408	−0.926	0.252	−2.067
I	0.20	1.816	−0.477	−0.913	0.248	−1.924
II	0.20	1.812	−0.483	−0.914	0.252	−1.983
I	0.25	1.871	−0.605	−0.831	0.252	−1.559
II	0.25	1.867	−0.591	−0.827	0.256	−1.608
I	0.30	1.923	−0.642	−0.707	0.260	−1.118
II	0.30	1.920	−0.650	−0.691	0.258	−1.127
I	0.50	2.011	−0.311	−0.307	0.258	−0.020
II	0.50	2.015	−0.302	−0.311	0.256	−0.005

seen from Fig. 6 where we plot mean-wall separation $\langle h^* \rangle$ (a) and $-\tau_{\|}^*$ (b) as functions for T^* at $\tau_3^*=-0.24$ and $\alpha=0.0$. Both plots comprise two branches. In the "low"-temperature regime up to $T^*=1.6$, $\langle h^* \rangle$ increases linearly with a very small slope $g^{(2)}$ for the one-layer vicinal phase has solidlike character throughout this regime. Since $\langle h^* \rangle$ changes very little with temperature up to $T^*=1.6$, $\tau_{\|}$ depends strongly on T and decreases linearly, as expected for an elastic solid. Somewhere in the vicinity of $1.60<T^*<1.64$ the pore solid melts abruptly. $g^{(2)}$ establishes the fluidlike nature of the new phase at $T^*=1.64$. Within the infinite resolution of our plots, it appears that constant load, zero shear strain melting is discontinuous (i.e., a first-order phase transition). For the "high"-temperature branch ($T^*>1.64$) $\langle h^* \rangle$ increases monotonically and highly nonlinearly. Simultaneously $\tau_{\|}$ decreases nearly linearly, but with a

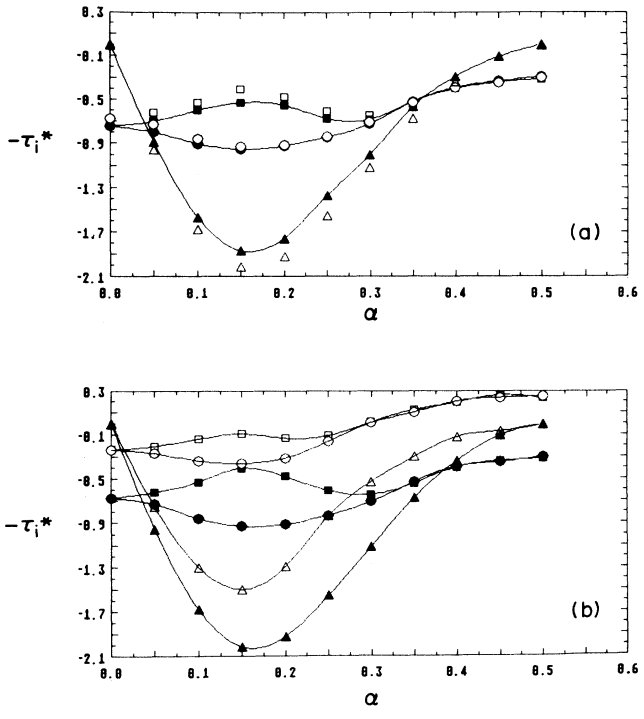

FIG. 5. Negative stress components $-\tau_i^*$ as functions of α. (a) $\tau_3^*=0.0$, $T^*=1.00$: $-\langle \tau_1^* \rangle$(■); $-\langle \tau_2^* \rangle$(●); $-\langle \tau_4^* \rangle$(▲). $\tau_3^*=-0.24$, $T^*=1.00$: $-\langle \tau_1^* \rangle$(□); $-\langle \tau_2^* \rangle$(○); $-\langle \tau_4^* \rangle$(△). (b) $\tau_3^*=-0.24$, $T^*=1.00$: $-\langle \tau_1^* \rangle$(■); $-\langle \tau_2^* \rangle$(●); $-\langle \tau_4^* \rangle$(▲). $\tau_3^*=-0.24$, $T^*=1.25$: $-\langle \tau_1^* \rangle$(□); $-\langle \tau_2^* \rangle$(○); $-\langle \tau_4^* \rangle$(△). Full lines from cubic spline fit are intended only to guide the eye.

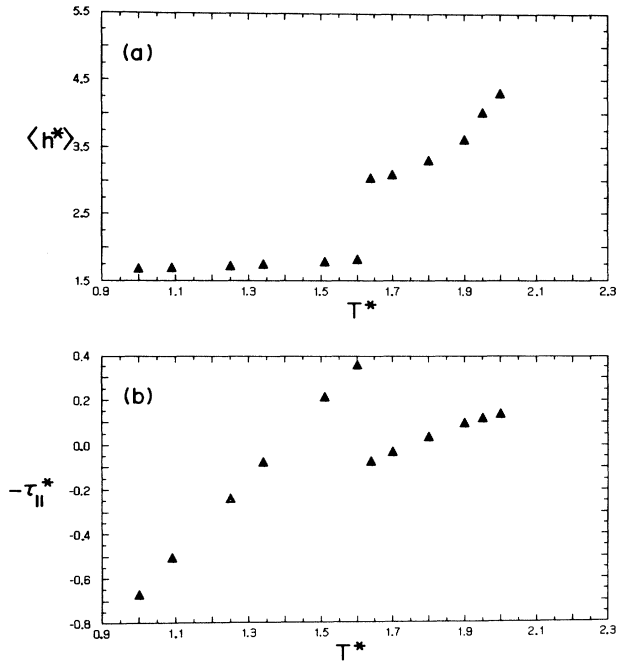

FIG. 6. (a) Average wall separation $\langle h^* \rangle$ as a function of T^* at $\alpha=0.0$, $\tau_3^*=-0.24$. (b) $-\tau_{\|}^*=-(\langle \tau_1^* \rangle+\langle \tau_2^* \rangle)/2$ as a function of T^* at $\alpha=0.0$, $\tau_3^*=-0.24$.

distinctly smaller slope than the "low"-temperature branch ($T^* \leq 1.60$), which is not surprising for a dense liquidlike phase.

Since $g^{(2)}$ merely reflects the average local order in the arrangement of molecules, it cannot *per se* be used to distinguish between a fluid phase (wherein the molecules are mobile) and a rigid disordered medium (i.e., glass). To verify that the atoms indeed become mobile as the vicinal solid is sheared, we computed the lateral components of their mean-square displacements (MSD) by microcanonical ensemble MD, where N,h,E, and α are fixed parameters. The details of the MD procedure are given elsewhere.[29] During the period 2 ps $< t <$ 6 ps, the MSD obeys a power-law Ct^d, where C and d are constants. For $0.0 < \alpha < 0.3$ the MSD rises rapidly to a plateau, remaining constant over this period (i.e., $d = 0$). For $0.3 < \alpha < 0.5$, on the other hand, d is positive and increases with α. At $\alpha = 0.5$, $d \simeq 1.0$ and the value of $D = C/2$ is comparable to that of the diffusion coefficient of the bulk fluid. The onset of diffusion, which appears continuous within the constraints dictated by the resolution of α and the precision of numerically determined values of d, parallels the transition in character of $g^{(2)}$ from sharply oscillatory to smooth (see Fig. 3).

VII. SUMMARY AND DISCUSSION

In this article we investigate melting of a solid monolayer confined between two solid walls. The isostress-isostrain Monte Carlo technique, in which N, τ_3, T, and α are fixed, along with the complementary strains, is applied to the prototypic slit pore (a monatomic fluid confined between plane parallel walls consisting of like atoms fixed in the fcc(100) configuration). Shear melting of the monolayer is effected by increasing α from 0 (where the vicinal phase is strictly solid) at fixed N, τ_3, and T. When α exceeds a critical value, the monolayer begins to melt. The melting is a continuous transition, which yields a disordered molten phase. The continuous nature of shear melting is qualitatively unaffected by changes in either load or temperature. On the other hand, when T is increased at constant N, τ_3, and α, the monolayer melts within a narrow temperature range. Normal thermally induced melting thus appears to be a first-order transition.

Since N is fixed in the isostress-isostrain ensemble, shear melting occurs without drainage. This is not so in the grand-canonical ensemble, where T, μ, and h are fixed parameters. When strained in this ensemble the vicinal solid responds elastically until a critical strain is reached. If the solid is strained further, a molten phase forms with concomitant drainage (i.e., an entire layer of atoms escapes from the pore). Neither the (N,τ_3,T) nor the (μ,h,T) ensemble is suitable for mimicking the actual SFA, in which the walls are slid at constant T with the vicinal phase in contact with bulk fluid, that is, with μ fixed. Therefore, to simulate shear melting under constraints more closely resembling the conditions under which the SFA operates, one should use some sort of grand ensemble in which μ and T are fixed parameters. The question remains: which additional independent thermodynamic state variables should be taken as fixed ensemble parameters, analogous to the complementary strains σ_1, σ_2, and σ_4, which are the additional parameters of the (N,τ_3,T) ensemble used in this work? The ideal choice of variables would of course be those actually controlled by the SFA. However, in the real apparatus the walls are attached to springs, which in turn are connected to points whose positions are manipulated. Hence neither the stresses nor the strains on the vicinal phase itself are *directly* controlled, but rather the *strains* on the *composite* system comprising the vicinal phase plus attached springs. For a given setting of the laboratory fixed points of attachment (or equilibrium positions) of the springs, the stresses τ_3 and τ_4 (and, in general, the y component of the shear stress, $\tau_5 = T_{yz}$) acting on the walls can be determined from a knowledge of the isothermal elastic constants of the (assumed Hookean) springs and the measured strains of the springs. The complete set of thermodynamic variables controlled by the SFA is μ, τ_3, T, and τ_4 plus the remaining complementary strains σ_1 and σ_2. The appropriate ensemble in which to describe the vicinal phase itself is therefore that particular grand-isostress ensemble wherein the fixed parameters are just these variables.

ACKNOWLEDGMENTS

This work has been supported by the U.S. Department of Energy under Grant No. DE-FG02/85ERG0310 and the United States Army Research Office under Grant No. OAAL03-90-G-0074. D. J. Diestler and M. Schoen gratefully acknowledge a travel grant from NATO (CRG801927). Computations have been carried out on the ETA 10P at the Purdue University Computing Center and on the CRAY Y-MP/832 of the Höchstleistungsrechenzentrum at Forschungszentrum Jülich. We thank both institutions for generous allowances of computer time.

*Present address: Department of Agronomy, University of Nebraska, Lincoln, NE 68583

[1] J. E. Shigley, *Mechanical Engineering Design* (McGraw-Hill, New York, 1977).
[2] P. F. Low, Langmuir **3**, 181 (1987).
[3] F. M. Etzler and W. Drost-Hansen, in *Advances in Chemistry Series,* No. 188, edited by M. Blank (American Chemical Society, Washington, DC, 1980), p. 486.
[4] J. N. Israelachvili and P. M. McGuiggan, Science **241**, 795 (1988).
[5] J. Israelachvili, P. McGuiggan, M. Gee, A. Homola, M. Robbins, and P. Thompson, J. Phys.: Condens. Matter **2**, SA89 (1990).
[6] S. Granick, Science **253**, 1374 (1991).
[7] R. Evans, Adv. Phys. **28**, 143 (1979).
[8] Y. Zhou and G. Stell, Mol. Phys. **66**, 767 (1989).
[9] J. E. Lane and T. H .Spurling, Aust. J. Chem. **29**, 2103 (1974).
[10] I. K. Snook and W. van Megen, J. Chem. Phys. **72**, 2907

(1980).
[11]M. Schoen, D. J. Diestler, and J. H. Cushman, J. Chem. Phys. **87**, 5464 (1987).
[12]C. L. Rhykerd, Jr., M. Schoen, D. J. Diestler, and J. H. Cushman, Nature (London) **330**, 461 (1987).
[13]M. Schoen, C. L. Rhykerd, Jr., D. J. Diestler, and J. H. Cushman, Scinece **245**, 1223 (1989).
[14]P. A. Thompson and M. O. Robbins, Phys. Rev. A **41**, 6830 (1990).
[15]P. A. Thompson and M. O. Robbins, Science **250**, 792 (1990).
[16]M. L. Gee, P. M. McGuiggan, and J. N. Israelachvili, J. Chem. Phys. **93**, 1895 (1990), and references therein.
[17]J. N. Israelachvili, P. M. McGuiggan, and A. M. Homola, Science **240**, 189 (1988).
[18]M. Lupkowski and F. van Swol, J. Chem. Phys. **95**, 1995 (1991).
[19]H. Callen, *Thermodynamics* (Wiley, New York, 1966), Chap. 13.
[20]D. C. Wallace, *Thermodynamics of Crystals* (Wiley, New York, 1972), Chap. 2.
[21]J. H. Weiner, *Statistical Mechanics of Elasticity* (Wiley, New York, 1983), Chap. 1.
[22]E. Schrödinger, *Statistical Thermodynamics* (Dover, New York, 1989), Chap. 2.
[23]T. L. Hill, *An Introduction to Statistical Thermodynamics* (Dover, Nw York, 1986), Chap. 1.
[24]D. A. McQuarrie, *Statistical Mechanics* (Harper and Row, New York, 1976), Chap. 2.
[25]P. N. Vorontsov-Vel'yaninov, A. M. El'yashevich, L. A. Morgenshtern, and V. P. Chasovskikh, High Temp. (USSR) **8**, 261 (1970).
[26]J. E. Finn and P. A. Monson, Mol. Phys. **65**, 1345 (1988).
[27]N. Metropolis, A. W. Rosenbluth, M. N. Rosenbluth, A. H. Teller, and E. Teller, J. Chem. Phys. **21**, 1087 (1953).
[28]M. P. Allen and D. J. Tildesley, *Computer Simulation of Liquids* (Clarendon, Oxford, 1987).
[29]M. Schoen, J. H. Cushman, D. J. Diestler, and C. L. Rhykerd, Jr., J. Chem. Phys. **88**, 1394 (1988).